IJRCS

International Journal of Robotics and Control Systems
Vol. 2, No. 3, 2022, pp. 477-491
ISSN 2775-2658
http://pubs2.ascee.org/index.php/ijrcs

ASCEE

A Simple Method for Stator Inductance and Resistance Estimation for PMSM at Standstill

Justas Dilys [a,b,1,*], Voitech Stankevič [a,b,2]

[a] State Research Institute Center for Physical Sciences and Technology, 02300 Vilnius, Lithuania
[b] Vilnius Gediminas Technical University Faculty of Electronics, Naugarduko 41, LT-03227 Vilnius, Lithuania
[1] justas.dilys@ftmc.lt; [2] voitech.stankevic@ftmc.lt
[*] Corresponding Author

ARTICLE INFO

Article History
Received May 02, 2022
Revised July 12, 2022
Accepted July 20, 2022

Keywords
dq inductances;
Resistance;
Standstill;
PMSM

ABSTRACT

An accurate stator resistance and inductance are necessary for high-performance permanent magnet synchronous motor (PMSM) control. The stator resistance and inductance can be estimated during motor standstill operation. This study proposes a standstill estimation method for the determination of dq-axis inductances and resistance of a PMSM drive system fed by a conventional voltage source inverter (VSI). The proposed method estimates both inductance and the rotor's position using the same algorithm, and knowledge of its initial position is not required. The d- and q-axis inductances were estimated by applying three short-time voltage pulses and measuring phase current peak values. The stator's resistance is estimated by monitoring the exponential decay process of the direct axis current. The method was verified by simulation and experiments conducted on two different PM synchronous motors. A good agreement of simulation and experimental results was obtained. Moreover, the proposed method is relatively simple and can identify stator resistance and inductance at any motor load condition. Compared to the existing parameter estimation strategies, the proposed estimation scheme has a relatively faster estimation time. Additionally, it is shown that the method accounts for the dead-time effect as well.

1. Introduction

The permanent magnet synchronous motor has become extremely popular, and the most obvious choice in many applications due to its inherent advantages like higher efficiency, higher torque to weight ratio, smaller size, etc. [1]. Using rare-earth permanent magnets enhances the magnetic flux density in the air gap and increases the power density and torque density of PMSMs. Therefore, the majority of automotive manufacturers choose PMSMs as the traction motor in their vehicles [2].

Accurate offline identification of stator resistance and inductance is necessary for proper tuning of the system controller [4, 5], the position based on electromotive force (EMF) [6] or the based model [7], the parameters should be obtained before motor startup, otherwise, the performance of driver will be poor. Moreover, parameter identification at standstill is essential for applications with load machinery connected, since it is not permissible to make the rotor deviate from the initial position during estimating parameters [8]. According to the operation status in the voltage source inverter (VSI) based parameter identification system, the methods can be divided into two classes: the offline and online identification methods [9]. The online estimation techniques [10, 11] are conducted while

the PMSM is in operation; this method can estimate the PMSM parameters without disturbing its operation. However, the offline d- and q-axes inductance parameters in the online identification method are still necessary before the motor startup to guarantee the motor's regular operation [12].

To experimentally compute machine parameters, the academic literature proposes several methods for both standstill and rotational tests (offline). Rotational tests, while being popular and accurate, require a special test rig and an external prime mover for the Motor Under Test (MUT). Standstill tests can be performed on either a blocked or a free-to-spin rotor [3].

A lot of offline methods have already been proposed to identify the inductance and resistance parameters [8, 13, 14, 15, 16, 12, 17, 18, 19, 20]. The methods [8, 13] identify d- and q-axis inductances and stator resistance considering inverter nonlinearities; however, additional initial rotor position estimation algorithm is required. Inductance identification methods with sequence pulse injection has been proposed [12], these techniques require a regression process, based on the fitting method. The discrete standard orthogonal polynomial with a look-up table is used to reduce computation complexity. A high frequency (HF) signal injection, which is superimposed on the fundamental excitations, is employed for inductance parameter identification [18, 17]. In [17] the least square identification method to obtain a linear model, however, lacks experimental validation. In [18], the rotor position and phase inductances are calculated by line-to-line voltage injection or d- and q-axis voltage injections. Offline inverter-nonlinearity-immune dq-axis inductance identification method based on the equivalent inductance model is proposed in [19]. Where [19] the equivalent resistance of the inverter nonlinearity is not contained in the inductance identification process, which need not be considered at all in the proposed method and the magnetic saturation and the cross saturation are considered.

In this article, the stator dq-axis inductances and resistance estimation method with only three short-time duration rectangular voltage pulses is presented. The main innovation of this method is that initial rotor position and motor parameters at standstill are estimated at same time applying the minimal voltage pulse count to the motor and making the estimation method very fast. The initial rotor position and motor parameters at standstill are estimated by measurement of the peak current values which depend on the rotor position. The proposed method is based on the VSI system; no extra auxiliary equipment is needed and rotor locking is not required. Because, the proposed method is valid under small phase currents it did not account magnetic saturation effect. Moreover, the presented method shows high accuracy, at the same time requiring very little computation power, and can be implemented in most microcontrollers. In this paper, the presented method is theoretically described and verified both by simulation and experiments performed on different PM motors.

2. PMSM model

A model of PM motor currents in rotor rotating reference frame is represented as in [9]

$$\begin{aligned}
\frac{\mathrm{d}i_d}{\mathrm{d}t} &= -\frac{R_s}{L_d}i_d + \omega_e\frac{L_q}{L_d}i_q + \frac{v_d}{L_d} \\
\frac{\mathrm{d}i_q}{\mathrm{d}t} &= -\frac{R_s}{L_q}i_q - \omega_e\frac{L_d}{L_q}i_d - \omega_e\frac{\lambda_{pm}}{L_q} + \frac{v_q}{L_q} \\
\frac{\mathrm{d}\omega_e}{\mathrm{d}t} &= \frac{p}{2J}\left(T_e - \frac{2B}{p}w_e - T_L\right) \\
\frac{\mathrm{d}\theta}{\mathrm{d}t} &= \omega_e
\end{aligned} \tag{1}$$

where v_d and v_q are d- and q-axis stator voltages, respectively; i_d and i_q are d- and q-axis stator currents, respectively; λ_{pm} is the permanent magnet flux; ω_e is the electrical rotor speed; J is the rotor inertia, B is the viscous friction coefficient; T_e is the electromagnetic torque, and T_L is the load torque; p is the number of poles; θ electrical rotor position; L_d and L_q are d- and q-axis stator

inductances, respectively.

During standstill, the PMSM is in static position and $\omega_e = 0$. Hence, (1) can be simplified as

$$\begin{aligned} \frac{\mathrm{d}i_d}{\mathrm{d}t} &= -\frac{R_s}{L_d} i_d + \frac{v_d}{L_d} \\ \frac{\mathrm{d}i_q}{\mathrm{d}t} &= -\frac{R_s}{L_q} i_q + \frac{v_q}{L_q}. \end{aligned} \tag{2}$$

3. Space Vector Pulse Width Modulation

The space vector pulse width modulation (SVPWM) is one main and competent technique to modulate the voltage references (outputs of the control algorithm) into the switching sequence [21]. SVPWM is a better computational PWM technique for the three-phase VSI as it produces less distortion in output voltage and produces higher AC output voltage [22].

Fig. 1 shows the two-level VSI space vector diagram representing the switching state in the six sectors. There are 6 active vectors ($v_1 - v_6$) when voltage is impressed across the load, and two zero vectors v_0, v_7 when the machine terminals are shorted through the lower switches or upper switches, respectively. Each active vector ($v_1 - v_6$) has magnitude $2/3V_{dc}$ and is aligned in 1 of 6 possible positions and are $\pi/3$ angle apart each other as shown in Fig. 1. The zero vectors v_0, v_7 are shown in center.

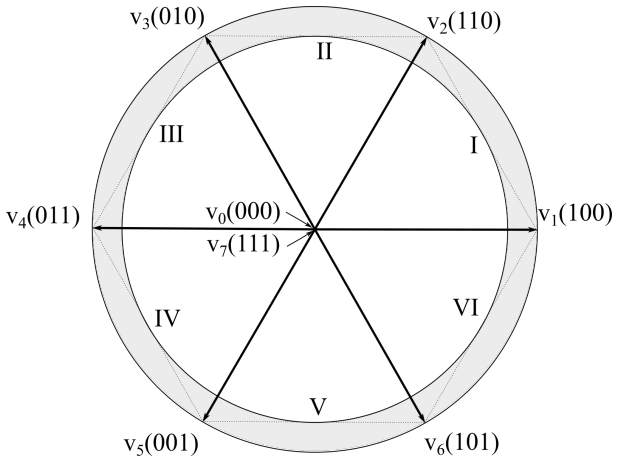

Fig. 1. Space vectors in three-phase voltage source inverter.

4. Method

During entire estimation time, only three short-time duration rectangular voltage pulses are applied to motor windings. Active vectors in time are separated by large inactive time, during inactive time the phase windings are not energized. During inactive time, the all phase windings could be connected to ground or not connected at all. Three active space vector pulse width modulation vectors $v_1(100)$, $v_3(010)$ and $v_5(001)$ are used in sequence as shown in Fig. 1.

The phase current distribution profiles diagram is shown in Fig. 2. Three-phase stationary currents i_a, i_b and i_c are measured with sensors. And two-phase dynamic currents i_d and i_q are calculated from stationary phase currents after the rotor position is estimated. The rotor position is estimated from three-phase stationary current's i_a, i_b and i_c as will be explained below.

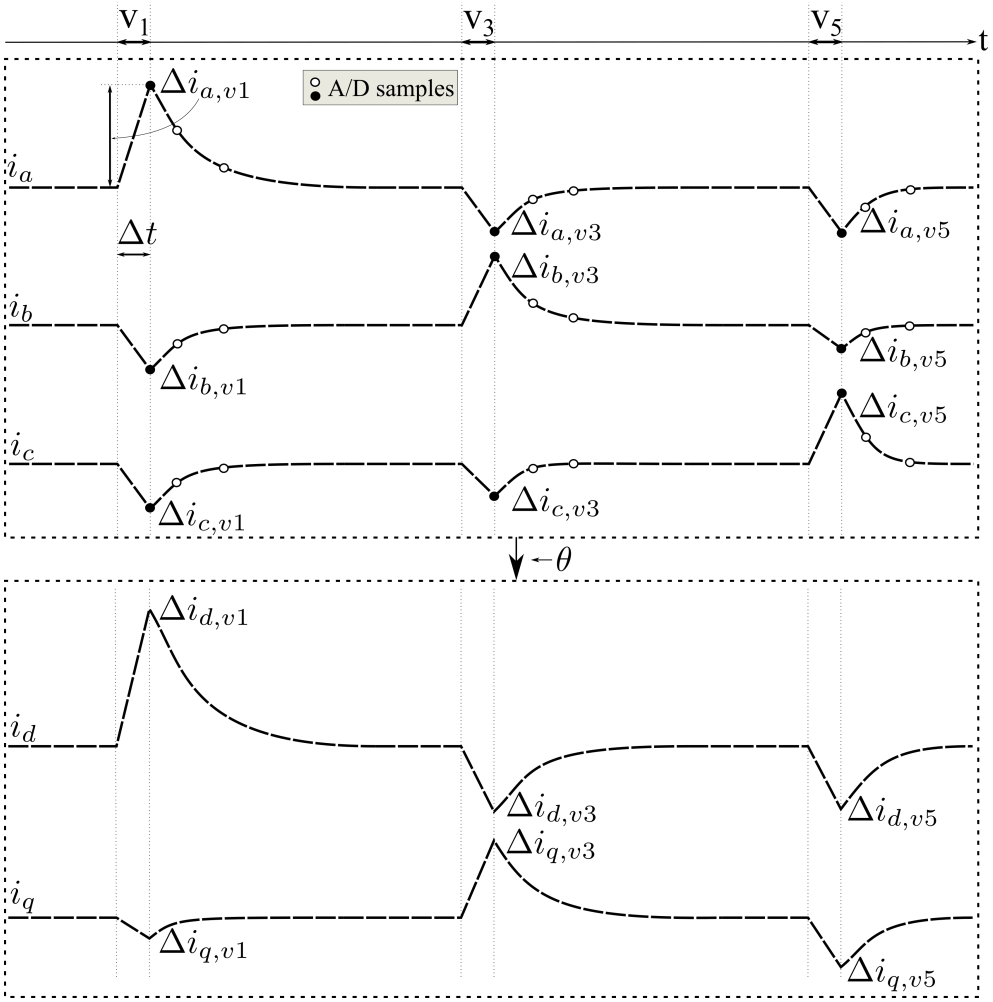

Fig. 2. Current distribution profiles

4.1. Initial Rotor Position Estimation

Because salient-pole PM motor inductance is in the form of $L_0 + L_2\cos(2\theta)$ where θ is rotor position at electrical angle, inductance L_0 is due to space fundamental air-gap flux and inductance L_2 due to rotor position [23], the equivalent admittance is in form $Y_0 + Y_2\cos(2\theta)$. In other word, the amplitude of the line current of the motor under excitation with a relative short time duration DC voltage is also a function of the rotor position given as in [23, 24]

$$\begin{aligned}
\Delta i_{a,v_1} &= i_0 + \Delta i_0\cos(2\theta) \\
\Delta i_{b,v_3} &= i_0 + \Delta i_0\cos\left(2\theta + \frac{2\pi}{3}\right) \\
\Delta i_{c,v_5} &= i_0 + \Delta i_0\cos\left(2\theta - \frac{2\pi}{3}\right)
\end{aligned} \tag{3}$$

where currents are phase peak values, i_0 is dc current component and Δi_0 is amplitude of a fluctuated component, obtained by properly connecting PM motor windings to supply voltages. The measurement of $\Delta i_{a,v_1}$ current the inverter a-phase is connected to DC supply and b- and c-phase to zero as shown in Fig. 3 or in other word, vector $v_1(100)$ are used, alternatively for $\Delta i_{b,v_3}$ - $v_3(010)$ and for $\Delta i_{c,v_5}$ - $v_5(001)$ as shown in Fig. 3.

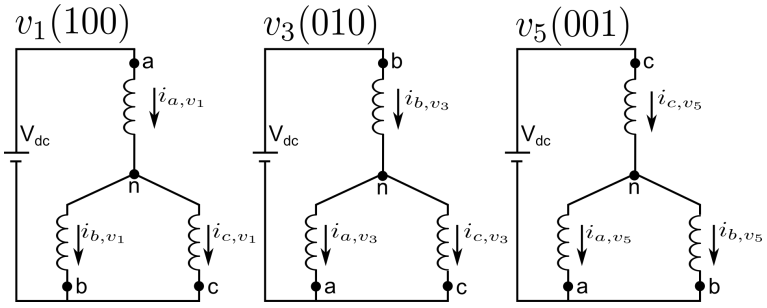

Fig. 3. Connection of PM motor at standstill for $\Delta i_a, \Delta i_b, \Delta i_c$ determination.

The above relation (3) is valid under the relatively small current, that is, the machine is not magnetically saturated [23]. Under the ideal case, where the current amplitude distribution is a sinusoidal function of the rotor position i_0, can be obtained as in [23, 24]

$$i_0 = \frac{1}{3}(\Delta i_{a,v_1} + \Delta i_{b,v_3} + \Delta i_{c,v_5}) \tag{4}$$

and signs of $\Delta\tilde{i}_a, \Delta\tilde{i}_b, \Delta\tilde{i}_c$ are obtained by

$$\begin{aligned}
\Delta\tilde{i}_a &= \Delta i_{a,v_1} - i_0 = \Delta i_0 \cos(2\theta) \\
\Delta\tilde{i}_b &= \Delta i_{b,v_3} - i_0 = \Delta i_0 \cos\left(2\theta + \frac{2\pi}{3}\right) \\
\Delta\tilde{i}_c &= \Delta i_{c,v_5} - i_0 = \Delta i_0 \cos\left(2\theta - \frac{2\pi}{3}\right).
\end{aligned} \tag{5}$$

After signs of $\Delta\tilde{i}_a, \Delta\tilde{i}_b, \Delta\tilde{i}_c$ are determined the relation between the rotor position and combination of signs can be summed up in Table 1.

Table 1. Relation between rotor position and signs of currents

$\theta \in$	sign($\Delta\tilde{i}_a$)	sign($\Delta\tilde{i}_b$)	sign($\Delta\tilde{i}_c$)	θ
$\left[-\frac{\pi}{12}; \frac{\pi}{12}\right)$	+	−	−	$\frac{\sqrt{3}}{2}\frac{\Delta\tilde{i}_c - \Delta\tilde{i}_b}{2\Delta\tilde{i}_a - \Delta\tilde{i}_b - \Delta\tilde{i}_c}$
$\left[\frac{\pi}{12}; \frac{3\pi}{12}\right)$	+	−	+	$\frac{\pi}{6} + \frac{\sqrt{3}}{2}\frac{\Delta\tilde{i}_a - \Delta\tilde{i}_c}{2\Delta\tilde{i}_b - \Delta\tilde{i}_a - \Delta\tilde{i}_c}$
$\left[\frac{3\pi}{12}; \frac{5\pi}{12}\right)$	−	−	+	$\frac{2\pi}{6} + \frac{\sqrt{3}}{2}\frac{\Delta\tilde{i}_b - \Delta\tilde{i}_a}{2\Delta\tilde{i}_c - \Delta\tilde{i}_a - \Delta\tilde{i}_b}$
$\left[\frac{5\pi}{12}; \frac{7\pi}{12}\right)$	−	+	+	$\frac{3\pi}{6} + \frac{\sqrt{3}}{2}\frac{\Delta\tilde{i}_c - \Delta\tilde{i}_b}{2\Delta\tilde{i}_a - \Delta\tilde{i}_b - \Delta\tilde{i}_c}$
$\left[\frac{7\pi}{12}; \frac{9\pi}{12}\right)$	−	+	−	$\frac{4\pi}{6} + \frac{\sqrt{3}}{2}\frac{\Delta\tilde{i}_a - \Delta\tilde{i}_c}{2\Delta\tilde{i}_b - \Delta\tilde{i}_a - \Delta\tilde{i}_c}$
$\left[\frac{9\pi}{12}; \frac{11\pi}{12}\right)$	+	+	−	$\frac{5\pi}{6} + \frac{\sqrt{3}}{2}\frac{\Delta\tilde{i}_b - \Delta\tilde{i}_a}{2\Delta\tilde{i}_c - \Delta\tilde{i}_a - \Delta\tilde{i}_b}$

After the region of rotor position has been determined, more precise rotor position can be determined. An expression for the rotor position can be generated by using trigonometric identities from the above expressions (5) and isolating the angle terms for θ and with approximation for small angles than $\theta \in \left[-\frac{\pi}{12}; \frac{\pi}{12}\right)$ the initial rotor position at standstill is as in [23, 24]

$$\theta \cong \frac{1}{2}\tan(2\theta) = \frac{\sqrt{3}}{2}\frac{\Delta\tilde{i}_c - \Delta\tilde{i}_b}{2\Delta\tilde{i}_a - \Delta\tilde{i}_b - \Delta\tilde{i}_c}. \tag{6}$$

The rotor position for other regions is given in Table 1. The above estimated initial rotor position is in range $\left[-\frac{\pi}{12}; \frac{11\pi}{12}\right)$ or π range. Because PM motor inductance is in the form of $L_0 + L_2\cos(2\theta)$ the period of inductance is π also, and further determination of polarity is not necessary.

4.2. dq-axis Inductance Estimation

The integral of (2) for i_d and i_q current for a short time duration Δt is the following

$$\begin{aligned}\int_0^{\Delta i_d} i_d \,\mathrm{d}i_d &= \int_0^{\Delta t}\left(-\frac{R_s}{L_d}i_d + \frac{v_d}{L_d}\right)\mathrm{d}t \\ \int_0^{\Delta i_q} i_q \,\mathrm{d}i_q &= \int_0^{\Delta t}\left(-\frac{R_s}{L_q}i_q + \frac{v_q}{L_q}\right)\mathrm{d}t.\end{aligned} \tag{7}$$

where Δi_d and Δi_q are produced currents. To integrate (7) we make assumption that current pulses start at zero, the phase is magnetically independent and linear, and that eddy currents in the motor laminations are negligible, the voltages v_d and v_q are constant values.

Applying above assumptions, the integral of i_d and i_q currents in (7) can be approximated as

$$\begin{aligned}\Delta i_d &\cong -\frac{R_s}{L_d}\frac{\Delta i_d \Delta t}{2} + \frac{v_d \Delta t}{L_d} \\ \Delta i_q &\cong -\frac{R_s}{L_q}\frac{\Delta i_q \Delta t}{2} + \frac{v_q \Delta t}{L_q}.\end{aligned} \tag{8}$$

Then the d- and q-axis inductances expression at standstill follows from (8) and are the following

$$\begin{aligned}L_d &\cong \frac{v_d \Delta t}{\Delta i_d} - \frac{R_s \Delta t}{2} \\ L_q &\cong \frac{v_q \Delta t}{\Delta i_q} - \frac{R_s \Delta t}{2}.\end{aligned} \tag{9}$$

Moreover, in expression (9) resistance voltage drop per phase can be eliminated. For enough short time Δt and from (9) it follows the inductance is in linear region [25]

$$\begin{aligned}L_d &\cong \frac{v_d \Delta t}{\Delta i_d} \\ L_q &\cong \frac{v_q \Delta t}{\Delta i_q}.\end{aligned} \tag{10}$$

At standstill then the motor currents and voltages are zero during a voltage pulse (v_1, v_3 or v_5) for a period of time Δt, then the all three-phase currents $\Delta i_a, \Delta i_b, \Delta i_c$ are measured for each voltage pulse, and knowing the rotor position θ, the motor currents in rotating reference frame for a vector v_i are

$$\begin{bmatrix} \Delta i_{d,v_i} \\ \Delta i_{q,v_i} \end{bmatrix} = \mathbf{C} \times \begin{bmatrix} \Delta i_{a,v_i} & \Delta i_{b,v_i} & \Delta i_{c,v_i} \end{bmatrix}^T \tag{11}$$

where v_i is v_1, v_3 or v_5 and transformation matrix [26]

$$\mathbf{C} = \frac{2}{3}\begin{bmatrix} \cos(\theta) & \cos\left(\theta - \frac{2\pi}{3}\right) & \cos\left(\theta + \frac{2\pi}{3}\right) \\ -\sin(\theta) & -\sin\left(\theta - \frac{2\pi}{3}\right) & -\sin\left(\theta + \frac{2\pi}{3}\right) \end{bmatrix}. \tag{12}$$

The motor voltages v_d and v_q are similarly calculated but instead of measuring phase voltages only DC link voltage V_{dc} are need and they are derived with the help of Fig. 3. Where for example

of vector v_1 phase voltages at stationary reference frame are: $v_{a,v_1} = \frac{2}{3}v_{dc}$, $v_{b,v_1} = v_{c,v_1} = -\frac{1}{3}V_{dc}$. Knowing the rotor position θ each stationary phase voltages are transformed into rotating reference frame

$$\begin{bmatrix} v_{d,v_i} \\ v_{q,v_i} \end{bmatrix} = \mathbf{C} \times \begin{bmatrix} v_{a,v_i} & v_{b,v_i} & v_{c,v_i} \end{bmatrix}^T \tag{13}$$

for each vector v_i: v_1, v_3 and v_5.

Having three sets of voltages v_{d,v_i}, v_{q,v_i} and currents i_{d,v_i}, i_{q,v_i} the phase inductances L_{d,v_i}, L_{q,v_i} can be estimated by (10) for each vector v_1, v_3 and v_5. The values v_{d,v_i}, v_{q,v_i} or i_{d,v_i}, i_{q,v_i} can be close to zero and division of small values can introduce large estimation errors. To overcome small values division problem, the assumption that at small-time period Δt the currents i_d and i_q are linear and v_d, v_q, L_d, L_q are constant values, the superposition principle can be used to express d- and q-axis inductances as

$$\begin{aligned} \hat{L}_d &\cong \frac{|v_{d,v_1}| + |v_{d,v_3}| + |v_{d,v_5}|}{|\Delta i_{d,v_1}| + |\Delta i_{d,v_3}| + |\Delta i_{d,v_5}|}\Delta t \\ \hat{L}_q &\cong \frac{|v_{q,v_1}| + |v_{q,v_3}| + |v_{q,v_5}|}{|\Delta i_{q,v_1}| + |\Delta i_{q,v_3}| + |\Delta i_{q,v_5}|}\Delta t. \end{aligned} \tag{14}$$

The modules of voltages and currents in (14) are taken because the sum of $v_{q,v_1} + v_{q,v_3} + v_{q,v_5}$ and $i_{q,v_1} + i_{q,v_3} + i_{q,v_5}$ is close to zero.

4.3. Stator Resistance Estimation

After releasing a supply voltage, the d- and q-axis current start to decay exponentially

$$\begin{aligned} i_d(t) &= \Delta i_{d,v_i} \mathrm{e}^{-t\frac{R_s}{L_d}} = \Delta i_{d,v_i} \mathrm{e}^{-\frac{t}{\tau_d}} \\ i_q(t) &= \Delta i_{q,v_i} \mathrm{e}^{-t\frac{R_s}{L_q}} = \Delta i_{q,v_i} \mathrm{e}^{-\frac{t}{\tau_q}} \end{aligned} \tag{15}$$

where t is time and τ_d, τ_q are time constants for d- and q-axis respectively. The time constant τ_d can be estimated by monitoring i_d current as well as τ_q by monitoring i_q current. It is important to monitor i_d, i_q phase currents decay because the decay time of stationary reference phase currents i_a, i_b, i_c are coupled related. The phase resistance $\hat{R}_s$ then can be estimated as

$$\hat{R}_s = \frac{\hat{L}_d}{\tau_d} = \frac{\hat{L}_q}{\tau_q}. \tag{16}$$

Having estimated rotor position θ the monitoring currents i_d and i_q can be obtained from measured stationary phase currents (i_a, i_b, i_c) and then transforming it into rotating reference frame using (13).

Because the rotor position is not know until three voltage pulses are applied, the stationary phase currents sample values have to be recorded into processor memory for each voltage pulse and then transformed into a rotating reference frame. However, for time constant τ_d or τ_q estimation, only two i_d or i_q respectively current sample points are needed. Any current i_d or i_q for exponential decay for any voltage vector pulse can be used, however, we prefer to use a vector which generate smallest i_q current amplitude and monitor i_d current decay, because of the smallest disturbance effect. The sample points schematic diagram are shown in Fig. 4.

The time t_d is delay time due to sample delay, times t_1 and t_2 are i_d current sample times after releasing supply voltage and the time difference of them is $t_{21} = t_2 - t_1$. Knowing two i_d current sample values and time difference of them the time constant $\hat{\tau}_d$ are estimated as

$$\hat{\tau}_d = \frac{t_2 - t_1}{\ln \frac{i_d(t_1)}{i_d(t_2)}} = \frac{t_{21}}{\ln \frac{i_d(t_1)}{i_d(t_2)}} \tag{17}$$

where $\ln$ is natural logarithm. From (17) we also see that estimated time constant $\hat{\tau}_d$ did not depend on sample delay time t_d.

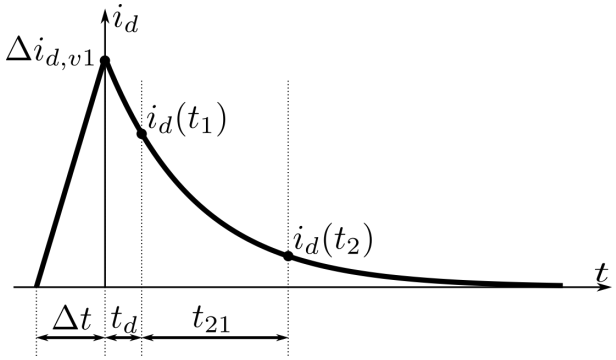

Fig. 4. The schematic diagram for exponential decay of i_d current.

4.4. Correction Step

The previously estimated inductances $\hat{L}_d$ and $\hat{L}_q$ using (14) is with the assumption that resistance voltage drop per phase are negligible due to short Δt period of time. To make estimation more accurate, a simple correction step to account resistance voltage drop per phase follows from (9) and is the following

$$\begin{aligned} \hat{L}_d^c &= \hat{L}_d - \frac{1}{2}\hat{R}_s \Delta t \\ \hat{L}_q^c &= \hat{L}_q - \frac{1}{2}\hat{R}_s \Delta t \end{aligned} \tag{18}$$

where $\hat{L}_d^c$ and $\hat{L}_q^c$ are corrected inductances.

Moreover, to account sample delay t_d, the (18) can be improved as well

$$\begin{aligned} \hat{L}_d^c &= \hat{L}_d \, \mathrm{e}^{-\frac{t_d}{\hat{\tau}_d}} - \frac{1}{2}\hat{R}_s \Delta t \\ \hat{L}_q^c &= \hat{L}_q \, \mathrm{e}^{-\frac{t_d}{\hat{\tau}_q}} - \frac{1}{2}\hat{R}_s \Delta t \end{aligned} \tag{19}$$

where unknown constant $\hat{\tau}_q$ can be found from (16) and is $\hat{\tau}_q = \hat{\tau}_d \hat{L}_q / \hat{L}_q$.

After inductances have been corrected using (19) or (18) the estimated stator resistance is corrected as well using (16). There for correction $\hat{L}_d^c$ inductance is used or briefly $\hat{R}_s^c = \hat{L}_d^c / \hat{\tau}_d$.

4.5. Schematic Diagram

A graphical representation of the proposed method is shown in Fig. 5, where active vector v_i is v_1, v_3 or v_5, and the sequence is always the same.

5. Experimental and Simulation Results

5.1. Simulation

To verify the presented algorithm mathematical accuracy of presented algorithm, a computer simulation is performed. Simulation of the PMSM1 given in Table 2 are performed with delay time $t_d = 0$ s. The phase currents waveforms are shown in Fig. 6(a) and Fig. 6(b) for all three voltages pulses. The PMSM initial position was set to $\theta = 1.23$ rad and estimated position $\hat{\theta} = 1.237$ rad. The d- and q-axis inductances estimated without correction step are $\hat{L}_d = 140.95$ μH and $\hat{L}_q = 211.21$ μH respectively, the resistance without correction step $\hat{R}_s = 0.0604$ Ω. After correction step, the final estimated inductance values are $\hat{L}_d^c = 140.34$ μH, $\hat{L}_q^c = 210.61$ μH and $\hat{R}_s^c = 0.0601$ Ω. Comparing estimated inductances (L_d, L_q) and resistance (R_s) of motor PMSM1 given in Table 2 can be seen

how accurate presented method performs. The simulation shows excellent accuracy of the presented method.

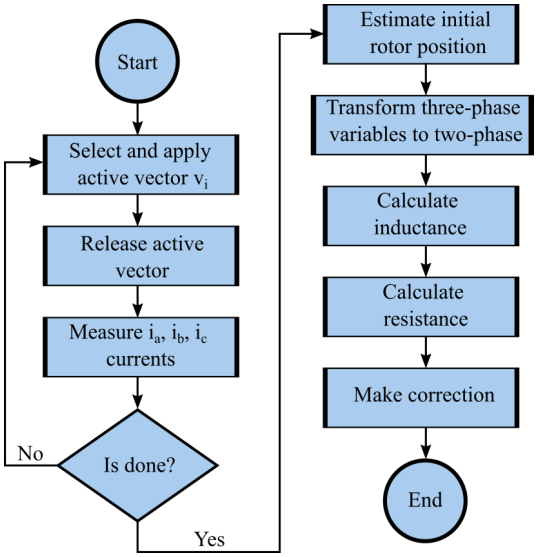

Fig. 5. Schematic diagram of the proposed method.

Table 2. Rated power and parameters of the two motors used in the tests

		PMSM1	PMSM2
Power supply voltage [V]	V_{dc}	24	24
Nominal power [W]	P_n	500	78
*Phase resistance [Ω]	R_s	0.06	0.38
*Inductance d-axis [μH]	L_d	140	145
*Inductance q-axis [μH]	L_q	210	180
Pole pair number	p	6	4

*_Note_. Parameters are measured using LCR meter.

5.2. Hardware Organization

The experimental system configuration is shown in Fig. 7. N channel metal oxide semiconductor field effect transistors (MOSFET) are used in this inverter for their low voltage drop and high speed. Microcontroller LPC1549 performs all necessary control processings. For current measurement, the three shunt current measurement technique is used. Because of current shunt connection type, the current of motor phase can be measured only then low transistor is on. The phase currents signal are amplified 10 times and are sampled by analog digital (A/D) converter of microcontroller LPC1549 using 12 bit resolution. The inverter is supplied by 24 V laboratory dc-voltage power source. Two different permanent magnet type brushless dc motor, whose specifications are given in Table 2, are used during experimental test.

5.3. Implementation

A specific gate switching modulation is implemented on LPC1549 microcontroller and shown in Fig. 8. The switching pattern is adopted to hardware, where phase currents can be measured only then low side transistor are on. The gate switching period T_s is selected large (30 ms) to enable decay energy after excitation. The voltage pulse time $\Delta t = 20$ μs are selected for all vectors v_1, v_3 and v_5.

The dead-time T_d are 700 ns selected for test inverter. A/D converter sample for peak currents starts after delay time T_w after all low side switches ($S\bar{a}$, $S\bar{b}$, $S\bar{c}$) are on. The time delay T_w are added to bypass switching noises and for test inverter $T_w = 4$ μs are selected. The sample time delay t_d account both dead-time and A/D delay and is $t_d = T_d + T_w$.

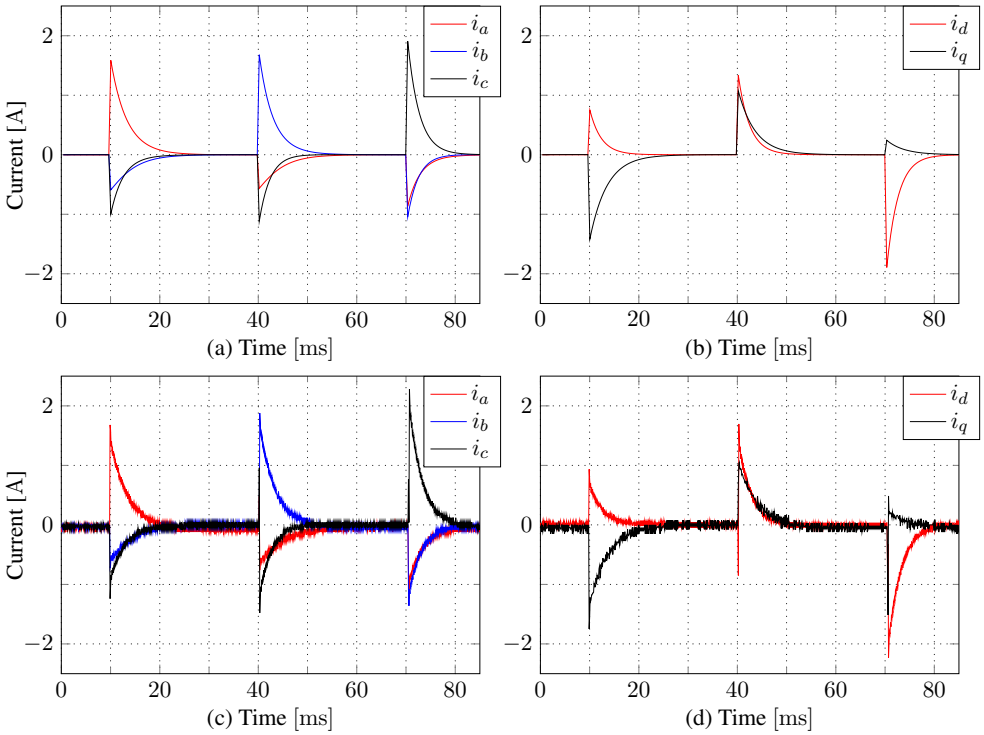

Fig. 6. Simulated and measured phase currents during estimation for PMSM1 at rotor position $\hat{\theta} = 1.23$ rad. (a) Simulation in stationary reference frame, (b) Simulation in rotating reference frame. (c) Measured in stationary reference frame, (d) Measured in rotating reference frame

5.4. Experimental Results

Experiments performed on two different motors with given parameters in Table 2. The currents build up during supply vector v_1 for PMSM1 motor are shown in Fig. 9. For illustrative purpose only, the rotor position is set to zero and estimated rotor position $\hat{\theta} = -0.05$ rad.

The transformed phase currents d and q into rotating reference frame are shown in Fig. 9(b), where i_q phase current vanish due to rotor position being at zero position. The phase current i_d increases from zero linearly to its peak value as shown in Fig. 9(b). The small current spikes at time 80 and 100 μs are due to switch commutation and took about 3 μs.

The phase currents during the whole estimation period for PMSM1 are shown in Fig. 6(c) and Fig. 6(d). The rotor position set randomly to any position and estimated $\hat{\theta} = 1.23$ rad. The d- and q-axis inductances estimated without correction step are $\hat{L}_d = 146.04$ μH and $\hat{L}_q = 215.97$ μH respectively, the resistance without correction step $\hat{R}_s = 0.057$ Ω. After correction step, the final estimated inductance values are $\hat{L}_d^c = 145.20$ μH, $\hat{L}_q^c = 214.80$ μH and $\hat{R}_s^c = 0.057$ Ω.

Fig. 10 illustrates the estimated stator values versus mechanical rotor position for PMSM1. Average values for d-axis inductance 145.69 μH and for q-axis 212.96 μH, average resistance value is 0.057 Ω for PMSM1. The maximum relative error for d-axis inductance is 3.0%, for q-axis inductance is 3.7% and for resistance is 5.5%.

The estimation results for PMSM1 with different dead-time delays are shown in Fig. 11. From the figure, we can see that the presented method accounts dead-time effect very well. The phase currents

during the whole estimation period for PMSM2 are shown in Fig. 12. The rotor position set randomly to any position and estimated $\hat{\theta} = 2.2$ rad. Because of higher stator resistance, the decay of PMSM2 are faster as we can see from Fig. 12 compared to Fig. 6(d). The final estimated inductance values are $\hat{L}_d^c = 144.72$ μH, $\hat{L}_q^c = 174.04$ μH and $\hat{R}_s^c = 0.37$ Ω.

Fig. 13 illustrates the estimated stator values versus mechanical rotor position for PMSM2. Average values for d-axis inductance 147.54 μH and for q-axis 178.05 μH, average resistance value is 0.35 Ω for PMSM2. The maximum relative error for d-axis inductance is 1.9%, for q-axis inductance is 2.1% and for resistance is 5.8% for PMSM2.

The maximum absolute deviation error (compared to nominal values) for d-axis inductance is 7.0%, for q-axis inductance is 4.5% and for resistance is 9.4% for PMSM1. And for PMSM2 d-axis inductance is 3.7%, for q-axis inductance is 2.8% and for resistance is 13.1%. In order to verify the effectiveness of the proposed method the results are compared with previous studies and are shown in Table 3. From the table, we can conclude that proposed method accuracy is very similar to previous studies.

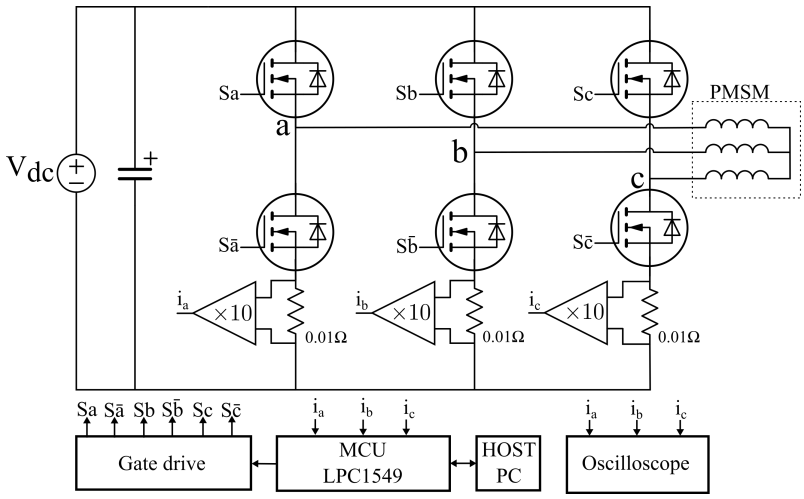

Fig. 7. Experimental system hardware organization.

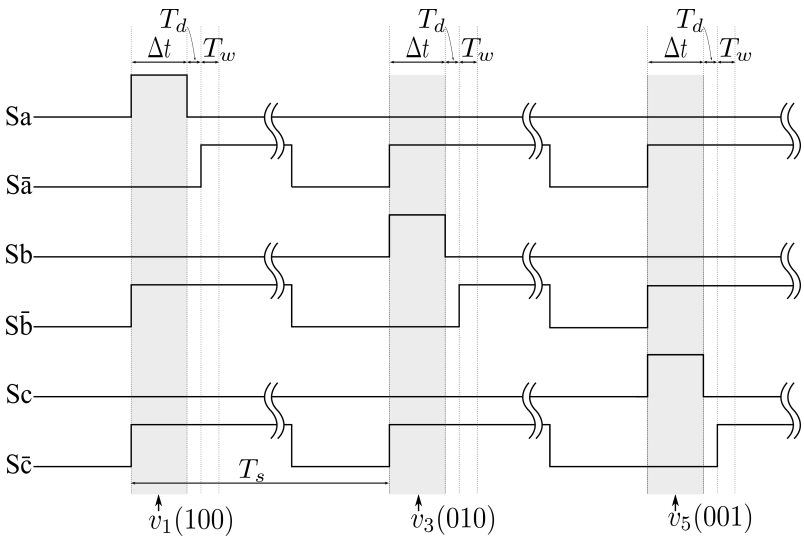

Fig. 8. The gate switching sequence.

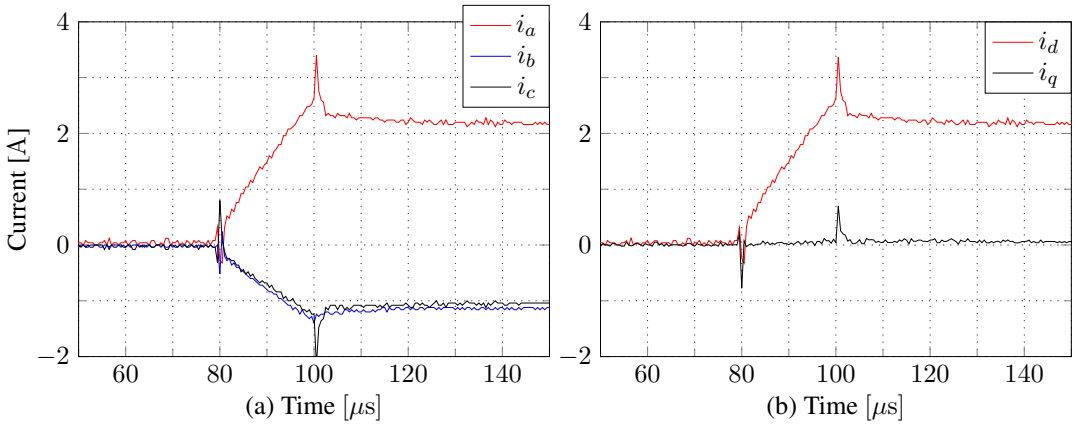

Fig. 9. Measured current linear build up during supply vector v_1 at estimated rotor position $\hat{\theta} = -0.05$ rad for PMSM1. (a) Stationary phase currents (b) d-axis and q-axis currents.

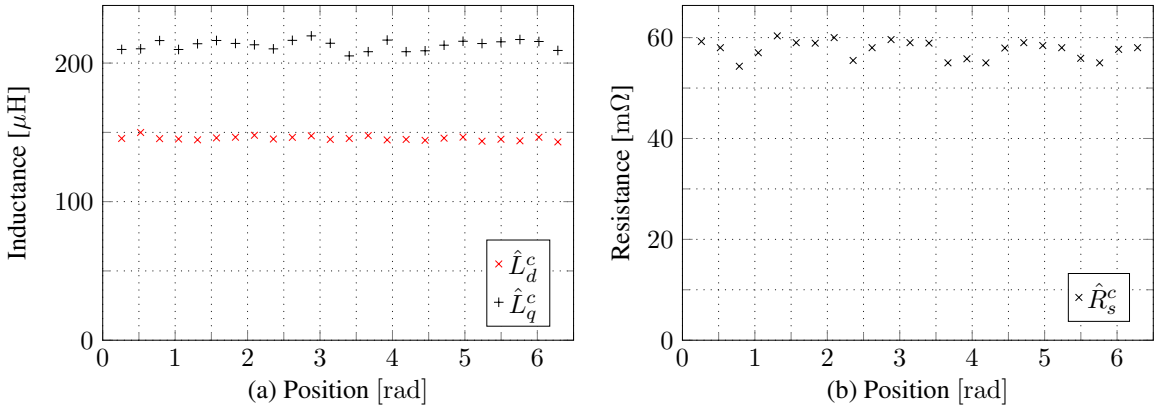

Fig. 10. Estimated stator values at different mechanical rotor positions for PMSM1 motor. (a) d and q-axis inductances, (b) Resistance.

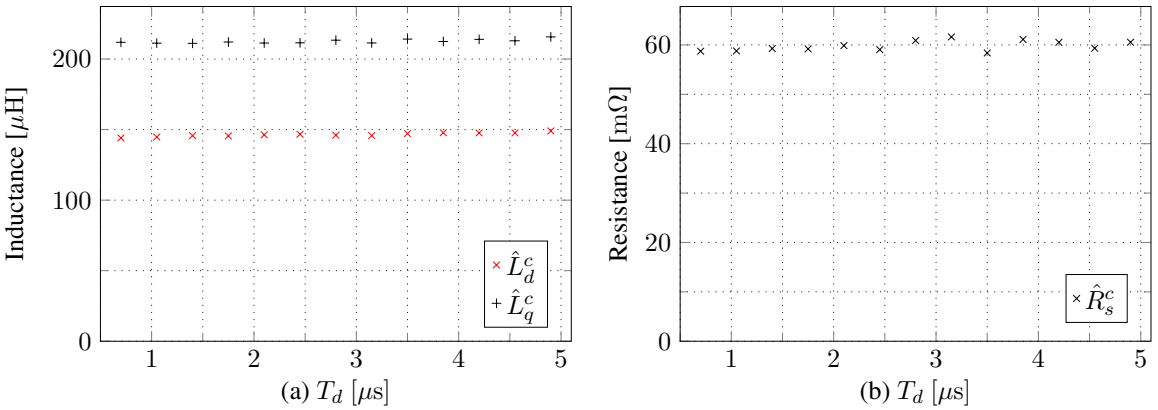

Fig. 11. Estimated stator values at different dead-time values for PMSM1 motor. (a) d- and q-axis inductances, (b) Resistance.

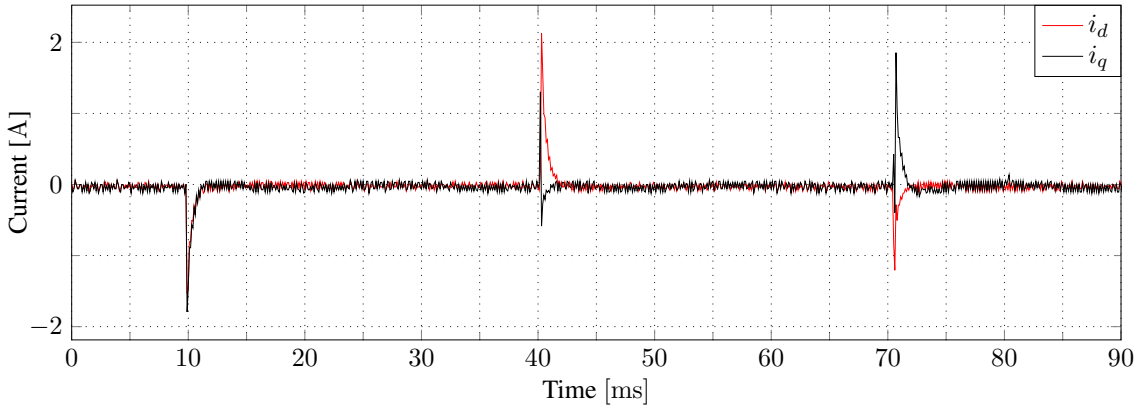

Fig. 12. Measured phase currents during estimation for PMSM2 at rotor position $\hat{\theta} = 2.2$ rad in rotating reference frame.

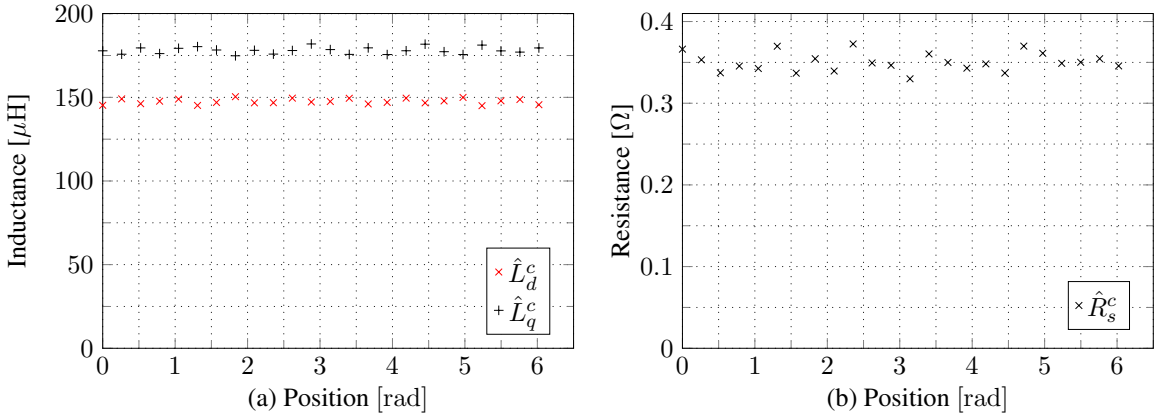

Fig. 13. Estimated stator values at different mechanical rotor positions for PMSM2 motor. (a) d- and q-axis inductances, (b) Resistance.

Table 3. Comparison of maximum identification errors of experimental results

Method	L_d	L_q	R_s	Comments
Proposed method	7.0%	4.5%	9.4%	PMSM1
Proposed method	3.7%	2.8%	13.1%	PMSM2
[19]	6%	6%	-	the rotor is locked
[14]	14.9%	13.3%	13.3%	-
[27]	12.4/3.6/5.7%	12.2/3.1/6.6%	-	depend on current
[12]	3.43%	2.68%	-	-
[18]	16%	16%	12/9%	depend on motor type
[13]	2.90%	12.77%	3.35%	need rotor position estimator

6. Conclusion

In summary, a simple method for identifying the stator's dq-axis inductance and resistance of PM synchronous motors at a standstill has been presented. The identification process is very fast and takes only part of the second. Moreover, the use of additional equipment is not needed. The tests of the motor can be performed with or without a locked rotor and do not require knowledge of its initial position. Such an estimation process does not require high computation power; therefore, it can be

used for low-cost, low-power embedded systems. The initial rotor position, as well as d- and q-axis inductances are estimated by applying three short-time voltage pulses and measuring phase current peak values. The stator's resistance is estimated by monitoring the exponential decay process of the i_d current. Finally, the inductances of the d- and q-axis are corrected, taking into account the stator's resistance and sampling delay. The method was verified by simulation and experiments conducted on two different PM synchronous motors. A good agreement with the reference PM models is obtained in all the cases. It is shown that the method accounts for the dead-time effect as well. Future research work will concern the extension of the study to the case of system magnetic saturation and cross saturation effect.

Author Contribution: All authors contributed equally to the main contributor to this paper. All authors read and approved the final paper.
Funding: This research received no external funding.
Conflicts of Interest: The authors declare no conflict of interest.

References

[1] S. Paitandi and M. Sengupta, "Analysis, fabrication and detailed comparative study of surface and interior rotor PMSM prototypes of identical nominal ratings and stators," Sādhanā, vol. 45, no. 1, Mar. 2020, https://doi.org/10.1007/s12046-020-1301-z.

[2] Y. Yang, S. M. Castano, R. Yang, M. Kasprzak, B. Bilgin, A. Sathyan, H. Dadkhah, and A. Emadi, "Design and Comparison of Interior Permanent Magnet Motor Topologies for Traction Applications," IEEE Transactions on Transportation Electrification, vol. 3, no. 1, pp. 86–97, Mar. 2017, https://doi.org/10.1109/tte.2016.2614972.

[3] V. Chandrasekaran, B. Jose, P. Mäki-Ontto, N. Mohan, K. Basu, and V. Giri, "Standstill Flux Linkage Measurement using Pulse Amplitude Modulated Current Injection towards Characterization of Interior Permanent Magnet Machines," 2022 IEEE Transportation Electrification Conference & Expo (ITEC), pp. 882-889, 2022, https://doi.org/10.1109/ITEC53557.2022.9813959.

[4] B. Sarsembayev, K. Suleimenov, and T. D. Do, "High Order Disturbance Observer Based PI-PI Control System With Tracking Anti-Windup Technique for Improvement of Transient Performance of PMSM," IEEE Access, vol. 9, pp. 66323–66334, 2021, https://doi.org/10.1109/access.2021.3074661.

[5] Z. Zhang, L. Jing, X. Wu, W. Xu, J. Liu, G. Lyu, and Z. Fan, "A Deadbeat PI Controller With Modified Feedforward for PMSM Under Low Carrier Ratio," IEEE Access, vol. 9, pp. 63463–63474, 2021, https://doi.org/10.1109/access.2021.3075486.

[6] Zhan, Z. Q. Zhu, and M. Odavic, "Nonparametric Sensorless Drive Method for Open-Winding PMSM Based on Zero-Sequence Back EMF With Circulating Current Suppression," IEEE Transactions on Power Electronics, vol. 32, no. 5, pp. 3808–3817, May 2017, https://doi.org/10.1109/tpel.2016.2592480.

[7] J. Dilys, V. Stankevič, and K. Łuksza, "Implementation of Extended Kalman Filter with Optimized Execution Time for Sensorless Control of a PMSM Using ARM Cortex-M3 Microcontroller," Energies, vol. 14, no. 12, p. 3491, Jun. 2021, https://doi.org/10.3390/en14123491.

[8] G. Wang, Y. Wang, J. Qi, R. Ni, W. Chen, and D. Xu, "Offline inductance identification of PMSM with adaptive inverter nonlinearity compensation," 2015 9th International Conference on Power Electronics and ECCE Asia (ICPE-ECCE Asia), Jun. 2015, https://doi.org/10.1109/icpe.2015.7168113.

[9] M. S. Rafaq and J.-W. Jung, "A Comprehensive Review of State-of-the-Art Parameter Estimation Techniques for Permanent Magnet Synchronous Motors in Wide Speed Range," IEEE Transactions on Industrial Informatics, vol. 16, no. 7, pp. 4747–4758, Jul. 2020, https://doi.org/10.1109/tii.2019.2944413.

[10] X. Ma and C. Bi, "A technology for online parameter identification of permanent magnet synchronous motor," CES Transactions on Electrical Machines and Systems, vol. 4, no. 3, pp. 237–242, Sep. 2020, https://doi.org/10.1016/j.measurement.2021.109342.

[11] S. Ye and X. Yao, "A Modified Flux Sliding-Mode Observer for the Sensorless Control of PMSMs With Online Stator Resistance and Inductance Estimation," IEEE Transactions on Power Electronics, vol. 35, no. 8, pp. 8652–8662, Aug. 2020, https://doi.org/10.1109/tpel.2019.2963112.

[12] X. Wu, X. Fu, M. Lin, and L. Jia, "Offline Inductance Identification of IPMSM With Sequence-Pulse Injection," IEEE Transactions on Industrial Informatics, vol. 15, no. 11, pp. 6127–6135, Nov. 2019, https://doi.org/10.1109/tii.2019.2932796.

[13] G. Wang, L. Qu, H. Zhan, J. Xu, L. Ding, G. Zhang, and D. Xu, "Self-Commissioning of Permanent Magnet Synchronous Machine Drives at Standstill Considering Inverter Nonlinearities," IEEE Transactions on Power Electronics, vol. 29, no. 12, pp. 6615–6627, Dec. 2014, https://doi.org/10.1109/tpel.2014.2306734.

[14] K. Liu and Z. Q. Zhu, "Determination of Electrical Parameters of PMSM Drive System at Standstill," 2016 IEEE Vehicle Power and Propulsion Conference (VPPC), Oct. 2016, https://doi.org/10.1109/vppc.2016.7791663.

[15] Q. Wang, G. Zhang, G. Wang, C. Li, and D. Xu, "Offline Parameter Self-Learning Method for General-Purpose PMSM Drives With Estimation Error Compensation," IEEE Transactions on Power Electronics, vol. 34, no. 11, pp. 11103–11115, Nov. 2019, https://doi.org/10.1109/tpel.2019.2900559.

[16] S. A. Odhano, R. Bojoi, S. G. Rosu, and A. Tenconi, "Identification of the magnetic model of permanent magnet synchronous machines using DC-biased low frequency AC signal injection," 2014 IEEE Energy Conversion Congress and Exposition (ECCE), Sep. 2014, https://doi.org/10.1109/ecce.2014.6953626.

[17] I. Omrane, E. Etien, O. Bachelier, and W. Dib, "A simplified least squares identification of permanent magnet synchronous motor parameters at standstill," IECON 2013 - 39th Annual Conference of the IEEE Industrial Electronics Society, Nov. 2013, https://doi.org/10.1109/iecon.2013.6699537.

[18] H.-C. Yeh and S.-M. Yang, "Phase Inductance and Rotor Position Estimation for Sensorless Permanent Magnet Synchronous Machine Drives at Standstill," IEEE Access, vol. 9, pp. 32897–32907, 2021, https://doi.org/10.1109/access.2021.3060774.

[19] Q. Wang, G. Wang, S. Liu, G. Zhang, and D. Xu, "An Inverter-Nonlinearity-Immune Offline Inductance Identification Method for PMSM Drives Based on Equivalent Impedance Model," IEEE Transactions on Power Electronics, vol. 37, no. 6, pp. 7100–7112, Jun. 2022, https://doi.org/10.1109/tpel.2021.3138886.

[20] G. Li, Z. Wu, S. Han, F. Jiang, T. Yang, and G. Wang, "Modified AC standstill method for PMSM $d-q$ axis inductances measurement," IET Science, Measurement & Technology, vol. 14, no. 4, pp. 430–434, Jun. 2020, https://doi.org/10.1049/iet-smt.2018.5499.

[21] J. Xu, M. Odavic, Z. Q. Zhu, Z.-Y. Wu, and N. Freire, "A Novel Space Vector PWM Technique with Duty Cycle Optimization through Zero Vectors for Dual Three-Phase PMSM," IEEE Transactions on Energy Conversion, 2022, https://doi.org/10.1109/tec.2022.3171705.

[22] G. N. Chethan and G. Kodeeswara kumaran, "Performance Analysis of PMSM Drive with SpaceVector PWM and Sinusoidal PWM fed VSI," 2019 International Conference on Power Electronics Applications and Technology in Present Energy Scenario (PETPES), Aug. 2019, https://doi.org/10.1109/petpes47060.2019.9003961.

[23] N. Matsui and T. Takeshita, "A novel starting method of sensorless salient-pole brushless motor," Proceedings of 1994 IEEE Industry Applications Society Annual Meeting, https://doi.org/10.1109/ias.1994.345475.

[24] M. Boussak, "Implementation and Experimental Investigation of Sensorless Speed Control With Initial Rotor Position Estimation for Interior Permanent Magnet Synchronous Motor Drive," IEEE Transactions on Power Electronics, vol. 20, no. 6, pp. 1413–1422, Nov. 2005, https://doi.org/10.1109/tpel.2005.854014.

[25] O. Safdarzadeh, M. Nezamabadi, and E. Afjei, "A precise method to detect the accurate rotor position in BLDC motors at standstill condition," 2016 7th Power Electronics and Drive Systems Technologies Conference (PEDSTC), Feb. 2016, https://doi.org/10.1109/pedstc.2016.7556835.

[26] Z. Q. Zhu, D. Liang, and K. Liu, "Online Parameter Estimation for Permanent Magnet Synchronous Machines: An Overview," IEEE Access, vol. 9, pp. 59059–59084, 2021, https://doi.org/10.1109/access.2021.3072959.

[27] P. Pescetto and G. Pellegrino, "Automatic Tuning for Sensorless Commissioning of Synchronous Reluctance Machines Augmented With High-Frequency Voltage Injection," IEEE Transactions on Industry Applications, vol. 54, no. 5, pp. 4485–4493, Sep. 2018, https://doi.org/10.1109/tia.2018.2839600.